Evaluation of the Mixing Performance of the Micromixers With Grooved or Obstructed Channels

Yeng-Yung Tsui[1]
e-mail: yytsui@mail.nctu.edu.tw

Ching-Shiang Yang

Chung-Ming Hsieh

Department of Mechanical Engineering,
National Chiao Tung University,
Hsinchu 300,
Taiwan R.O.C.

The mixing flows in microchannels were examined using numerical methods. To speed up fluid mixing, it is essential to generate lateral transport of mass. In this study, the mixing flow is disrupted by either placing grooves or block obstacles on the walls of the channels. Since the grooves or the blocks appear in a periodic configuration, the velocity is solved only in a section of the channel. With the repeating cycle of flow velocity field, the fluid concentration can be calculated throughout the entire length of the channel. Good agreement with experiments in the mixing performance justifies the present methodology. Two different channel configurations are under consideration: grooved channels and obstructed channels. The results reveal that with straight grooves, a well organized vortex flow is formed in the vertical plane along the groove, which leads to a helical flow in the channel. The mixing performance can be enhanced by having grooves on both the top and the bottom walls arranged in a staggered manner, by which the transversal velocity is largely increased. It is seen that the strength of the secondary flow and, thus, the mixing can be improved by suitably choosing geometric parameters of the groove, such as the depth, the width, and the oblique angle. It is also shown that the efficient mixing for the staggered herringbone type groove is due to the fluid stratification caused by the exchange of position of the resulted counter-rotating vortices. As for the obstructed channels, the flows are in essence two dimensional. Very strong transversal velocity can be produced by narrowing down the flow passage in the channel. However, the efficient mixing is obtained at the cost of large pressure head loss. [DOI: 10.1115/1.2948364]

1 Introduction

Rapid mixing is crucial to the microfluid systems, which are now widely used in biochemistry analysis, chemical synthesis, drug delivery, high-throughput screening, among others. In microsystems, the small size prohibits turbulent mixing. The Reynolds number is generally less than 100 and can be as low as 0.01, which lies in the creeping regime. Hence, the mixing in microchannels is predominantly governed by molecular diffusion. If the thickness of the lamella structure of the fluid is much larger than the characteristic diffusion length, it is difficult to obtain rapid mixing.

To enhance fluid mixing, either active or passive methods can be employed. Active mixing is usually achieved by periodically perturbing the flow field. A number of fluid actuation methods have been introduced, including electrokinetic force [1,2], ultrasonic actuation [3,4], thermal power [5,6], periodic pressure perturbation [7–9], etc. Active mixers have obvious disadvantages over passive mixers in the requirement of external power sources and the complexity in terms of fabrication, operation, maintenance, and package. On the other hand, passive mixers utilize no extra forcing mechanism other than the basic pressure head used to drive the fluid flow.

In smooth and regular flow fields, efficient mixing can be obtained by creating chaotic advection, which stretches and folds fluid elements [10,11]. According to chaotic advection theory, the chaos can arise in a nonlinear dynamic system provided that three degrees of freedom are present [12]. For two-dimensional flows, a time-dependent perturbation is usually imposed to provide the third degree of freedom to generate chaotic mixing. Under the condition of steady state, a three-dimensional flow is required. The active micromixers are of the former type, while the passive ones usually belong to the latter. Therefore, it is essential for the passive micromixers to generate strong enough lateral flows such that the fluid interface can be greatly stretched and folded.

Mengeaud et al. [13] examined a zigzag microchannel. Below a critical Reynolds number of about 80, the flow remains parabolic and the mixing is ensured by molecular diffusion. At high Reynolds numbers, a transversal velocity is induced due to the flow recirculation behind the sharp turning corners, which improves the mixing process. Similar results were observed in the study of Liu et al. [14] for square-wave channels. The flow field in these two types of micromixer is essentially two dimensional because the channels make sharp turns only on a plane. To create fully three-dimensional flow, Liu et al. [14] proposed a serpentine design by which the channel periodically makes sharp turning in a three-dimensional manner. It was shown that with this kind of microchannel the mixing ability is much improved over the square-wave channel for Reynolds numbers between 6 and 70. As an example, at a Reynolds of 70, the former produces 1.6 times more reacted phenolphthalein than the latter. However, the complex three-dimensional structure of the serpentine channel has posed a challenge to fabrication.

Another way to induce lateral transport is the use of patterned grooves on the wall surface of the channel [15]. It was schematically shown in the experimental study of Stroock et al. [16] that by placing straight grooves on the floor, a secondary flow is formed in transversal planes and the flow streamlines in the channel become helical. Similar transversal flows were also observed by Johnson et al. [17]. Instead of straight grooves, patterned grooves with herringbone structure result in a pair of counter-rotating helical flows. Chaotic advection can be generated by ar-

[1]Corresponding author.

Contributed by the Fluids Engineering Division of ASME for publication in the JOURNAL OF FLUIDS ENGINEERING. Manuscript received May 17, 2007; final manuscript received April 23, 2008; published online June 25, 2008. Assoc. Editor: Rajat Mittal.

ranging the herringbone grooves in a staggered manner: The direction of asymmetry of the herringbones switches with respect to the centerline of the channel from half a cycle to the other half. The results obtained by Stroock et al. [16] revealed that efficient mixing can be achieved for Reynolds numbers from 10^{-2} to 10.

To create corotating transversal flows, Kim et al. [18] placed barriers along the top surface of a channel while the floor was formed from ablated walls. The periodic insertion of the barriers leads to continuous exchange of flow pattern between the single vortex type and the double vortex type.

In the study of Howell et al. [19], two sets of straight grooves and two sets of chevron-shaped grooves appeared on both the top and bottom of the channel. The chevrons on the two walls direct in opposite directions. It was shown that due to the strengthened lateral velocities by the double grooves and the resulted complex vortex flows, the mixing is greatly enhanced.

To look into detailed flow behaviors and evaluate the mixing performance, it is required to visualize the flow field in the microchannel. Computational fluid dynamics is a good approach to fulfill this task and has been employed to examine different channel designs. For quantification of the mixing performance, either the particle tracking method or the transport equation method has been adopted. In the former, a number of particles are introduced into the channel and the positions of all particles are traced by using the Lagrangian approach. Because of the periodic configuration of the microchannel, the recording of the particle tracking can be used to generate the Poincare map to check if chaos occurs [9,20,21]. In the above studies, the particles are released at the inlet plane. By this means, the distribution of particles cannot be controlled; some regions in the outflow plane, especially near the walls, are often poorly covered by the particles seeded at the inflow plane. Mott et al. [22] developed a backtracking method in which the trace particles are introduced from the outlet plane. In this way, a uniform distribution of information across the entire outflow plane is obtained. A drawback of the Lagrangian approach is that the molecular diffusion is not taken into account. As for the other method, the distribution of the mass concentration for the mixed fluids is obtained by solving a transport equation [13,23,24]. This method requires that the grids used for calculation have sufficient resolution and the difference scheme must be of high order accuracy to avoid numerical diffusion. Comparing with the transverse dimension, the length of the channel is so long that most studies restrict their calculations to a short length due to enormous computational cost.

The present work aims at evaluating the mixing performance of different micromixers in full length of the channel. To take advantage of the periodic arrangement of the channel geometry, it is not necessary to solve for the velocity in the entire channel; only a section covering several periodic units is required to represent the velocity field. The transport equation for mass concentration is then solved throughout the full length of the channel by repeatedly making use of the periodic velocity field. This approach is applied to two types of micromixers (see Fig. 1). One is that with patterned grooves, including straight grooves and herringbone grooves, and in the other type the channel is partially obstructed by block obstacles. The use of block to disturb flow field is common in large-scale mixers and heat exchangers, but hardly found in micromixers.

2 Numerical Method

The flow field in the microchannels can be considered as steady and incompressible. The fluid density ρ, viscosity μ, and mass diffusivity D are assumed to be uniformly distributed, regardless of the different fluids used for mixing. The governing equations for mass, momentum, and concentration can be expressed as

$$\nabla \cdot \mathbf{V} = 0 \tag{1}$$

$$\nabla \cdot (\mathbf{V} \otimes \mathbf{V}) = -\nabla P + \frac{1}{\mathrm{Re}}\nabla^2 \mathbf{V} \tag{2}$$

$$\nabla \cdot (\mathbf{V}C) = \frac{1}{\mathrm{Pe}}\nabla^2 C \tag{3}$$

where $\mathbf{V}$ is the velocity vector and C the mass concentration. The above equations have been nondimensionalized using the mean velocity $\bar{U}$ and the channel height h as reference scales. The Reynolds number is defined by $\rho\bar{U}h/\mu$ and the Peclet number by $\bar{U}h/D$. The Peclet number and the Reynolds number are related by Pe=ReSc. Here, Sc is the Schmidt number defined by Sc $=\nu/D$, where ν is the kinematic viscosity.

To cope with the irregular geometry of the considered micromixers, a fully conservative finite volume method suitable for unstructured grid computation is utilized. The equations, being of divergence form as given in the above, are integrated over a control volume, which, in general, can be a polyhedron with arbitrary topology. With the use of the divergence theorem, the volume integrals of the convective and diffusive transports are transformed into surface integrals. The convective flux through the surface of the control volume is approximated by the second-order, nondiffusive central difference scheme. The use of central differencing is essential to the mixing computation because a scheme such as the upwind differencing possesses an inherent character of numerical diffusion. The numerical diffusion may overshadow physical diffusion during flow mixing. However, it is known that the central difference may result in oscillations in the solution. This causes serious problems in concentration calculation because it may exceed the limiting values of 0 and 1. Therefore, in the approximation of the convective flux for the concentration, we employ a blending strategy by which a weighting of 0.9 is assigned to the central difference and a weighting of 0.1 to the upwind difference. The diffusive flux is approximated by an over-relaxed approach [25,26]. This approach is applicable to a mesh with arbitrary shape and degenerates into the central difference form when the mesh is rectangular.

The governing equations are solved in a segregated manner. The nonlinearity of the equations and the coupling between them are treated in an iterative way. The momentum equation is solved first. The resulting velocities require adjustment and the pressure must be upgraded such that the mass is conserved. The enforcement of the continuity constraint brings about a pressure-correction equation. The pressure correction obtained by solving this equation is then used to correct the prevailing velocity and pressure fields. The same procedure is carried out repeatedly until convergence is achieved. After the velocity field is finalized, the distribution of fluid concentration is then sought by solving the corresponding transport equation. More details about the discretization and the solution method can be found in the studies of Tsui and Pan [25] and Tsui and Jung [26].

The heights of the microchannels are usually characterized by a dimension in the order of 100 μm, while the lengths are in the range of 3–5 cm. As a three-dimensional grid is constructed to cover these relatively long channels, millions of control volumes are required. This is an enormous burden to the computer resource.

As seen form Fig. 1, the grooves or obstacles appear periodically in the channel. To take advantage of the periodically varying geometry, the flow only in a periodic module is needed as the flow becomes fully developed. For periodic calculations, the same velocities must be imposed at the corresponding periodic boundaries. Particularly, a special treatment of the pressure field must be undertaken. It was first proposed by Patankar et al. [27] to decompose the pressure gradient into a periodic part and a linearly varying part. For a duct flow with a given mass flow rate, the linearly varying part of pressure gradient must be determined in an iterative manner [27–29]. Therefore, this procedure is time consuming

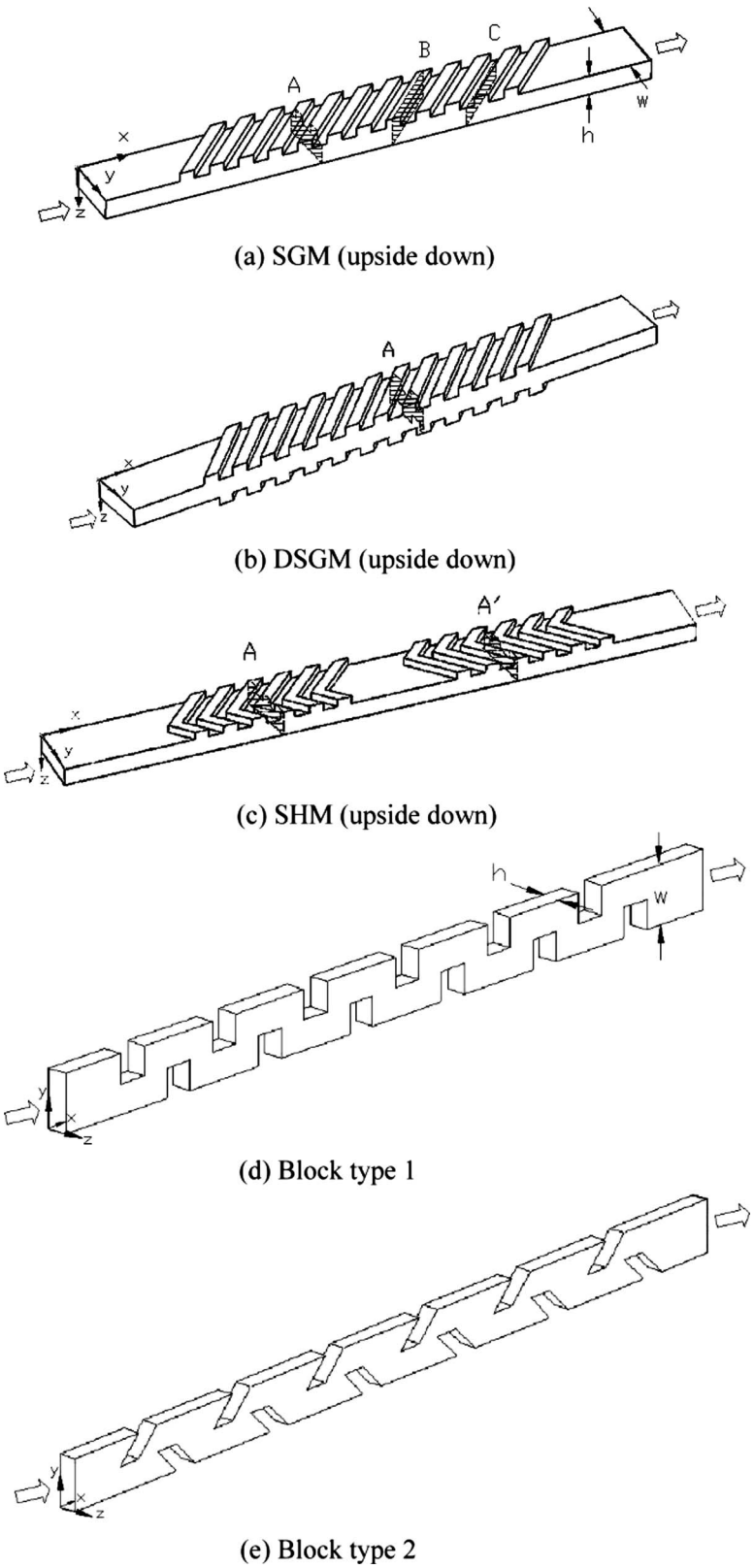

Fig. 1 Schematic drawings of the considered micromixers: (*a*) SGM, (*b*) DSGM, (*c*) SHM, (*d*) Block Type 1, and (*e*) Block Type 2

and modification on the existing computer code is required. In the present study, a simple procedure is used without bother of periodicity conditions. As an illustration, in calculating the velocity field for the straight groove micromixer (SGM), the computational domain comprises 12 grooves together with an entrance section at the beginning and an outflow section at the end (see Fig. 1(*a*)). In the simulation, a uniform velocity profile is prescribed at the inlet and the zero-gradient condition is imposed at the outlet. The re-

Table 1 Grid sizes for the meshes considered in the refinement tests for the SGM

	Cell number	Main passage	Groove
Mesh A	42,000	$\Delta x=\Delta y=\Delta z=0.1$	$\Delta x=\Delta y=\Delta z=0.1$
Mesh B	147,840	$\Delta x=\Delta y=\Delta z=0.07$	$\Delta x=\Delta y=0.07$ $\Delta z=0.03$
Mesh C	235,008	$\Delta x=\Delta y=\Delta z=0.06$	$\Delta x=\Delta y=0.06$ $\Delta z=0.026$
Mesh D	303,264	$\Delta x=\Delta y=\Delta z=0.055$	$\Delta x=\Delta y=0.055$ $\Delta z=0.024$

Table 2 Grid sizes for the meshes considered in the refinement tests for the SHM

	Cell number	Main passage	Groove
Mesh A	101,700	$\Delta x=\Delta y=\Delta z=0.1$	$\Delta x=\Delta y=\Delta z=0.1$
Mesh B	219,528	$\Delta x=\Delta y=\Delta z=0.08$	$\Delta x=\Delta y=0.08$ $\Delta z=0.04$
Mesh C	283,842	$\Delta x=\Delta y=\Delta z=0.07$	$\Delta x=\Delta y=0.07$ $\Delta z=0.036$
Mesh D	340,830	$\Delta x=\Delta y=\Delta z=0.06$	$\Delta x=\Delta y=0.06$ $\Delta z=0.03$

sulting velocity field in the grooved section becomes periodic and fully developed quickly. In order to get rid of the effects of the inlet and outlet, a section of seven grooves in the middle region is taken as a periodically repeating mixing cycle. The concentration field is then solved for by using the cyclic velocity field repeatedly until the required channel length is reached. As for the herringbone micromixer, 3 cycles of groove (each cycle comprises 12 grooves, as seen in Fig. 1(*b*)) are included in the velocity calculation and the velocity field in the second cycle is then used to compute mass mixing.

3 Results and Discussion

The simulated channels have a cross section with a height $h=70$ μm and a width $w=200$ μm ($w/h=2.86$). The total length of the channels is 3 cm ($l/h=428.6$). The width is the length scale in the y-direction and the height that in the z-direction. The x-, y- and z-axes are in the streamwise, spanwise, and cross stream (vertical) directions, respectively, which are defined in Fig. 1 for each type of microchannel considered. The Schmidt number used in the simulations is fixed at a value of 2×10^5. Thus, for a case with $\mathrm{Pe}=2\times10^5$, the Reynolds number is 1, while for $\mathrm{Pe}=2\times10^3$, the corresponding Reynolds number is 0.01.

The mixing performance is represented by the mixing index defined as

$$\sigma=\sqrt{\frac{1}{A}\sum_i (C_i-\bar{C})^2 A_i} \tag{4}$$

where C_i is the concentration at a computational cell with a cross-sectional area A_i, $\bar{C}$ an average of the concentration over the two fluids (=0.5 for the present study), and A the cross-sectional area of the channel. The summation is taken over all the cells in the cross section. The mixing index is 0.5 for completely segregated fluids and 0 for fully mixed fluids.

Grooved Micromixers. In order to validate the methodology described above, computations have been conducted to simulate the flows in a SGM and a staggered herringbone micromixer (SHM). The geometric configurations of the channels are taken from the study of Stroock et al. [16] Grid refinement tests were carried out to ensure the obtained solution being grid independent. Four different meshes, ranging from 96,900 cells to 621,108 cells for the SGM and from 319,200 cells to 1,053,360 cells for the SHM, were adopted in the tests. It is noteworthy that, as described previously, only a section in the middle is considered as a periodic cycle for concentration calculation. The numbers of cells for the meshes in 1 cycle are in the range of 42,000–303,264 for the SGM and in the range 101,700–340,830 for the SHM. The corresponding grid size is 0.1 h for the coarsest grid and about 0.024–0.06 h for the finest grid. The grid sizes for the different levels of mesh are given in Tables 1 and 2 for the SGM and SHM, respectively. Typical grid layouts used for the two types of mixer are shown in Fig. 2. Comparison with the experimental data of Stroock et al. for the flow with $\mathrm{Pe}=2\times10^5$, as shown in Fig. 3, indicates close resemblance between the two results. It can be seen that with the use of coarse meshes, the mixing rate is faster than that for the finer meshes and deviates more from the measurements. This result is not unexpected, based on the understanding that numerical diffusion is proportional to the grid size.

The groove-induced secondary velocity is usually weak, but is important to the mixing performance. Figure 4 presents the secondary flows in a cross section for the SGM and SHM. Also included is that for a double straight groove micromixer (DSGM) in which the grooves appear on both the bottom wall and the top wall in a staggered way to each other (see Fig. 1(*b*)). In the grooves, the flow field is characterized by a lateral flow from the right to the left in Fig. 4(*a*) for the SGM. More important is that there exists a transversal velocity flowing in the opposite direction

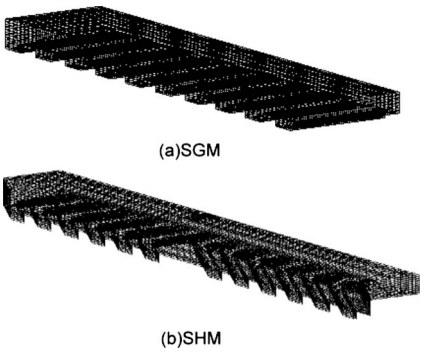

Fig. 2 Typical grid layouts used for (*a*) SGM and (*b*) SHM

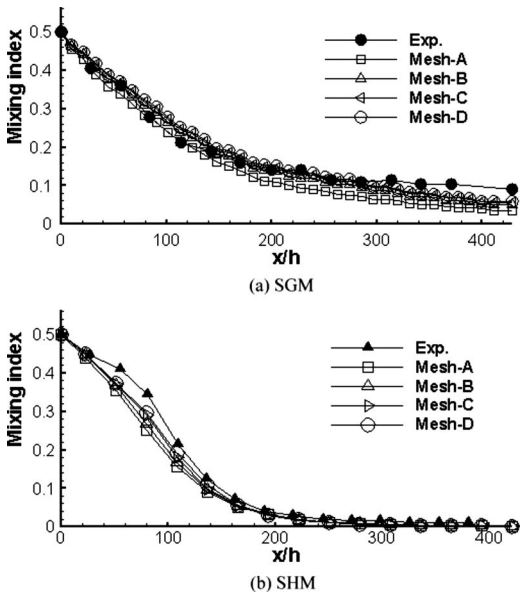

Fig. 3 Comparison of the predicted mixing indices with experiments using different meshes for (*a*) SGM and (*b*) SHM

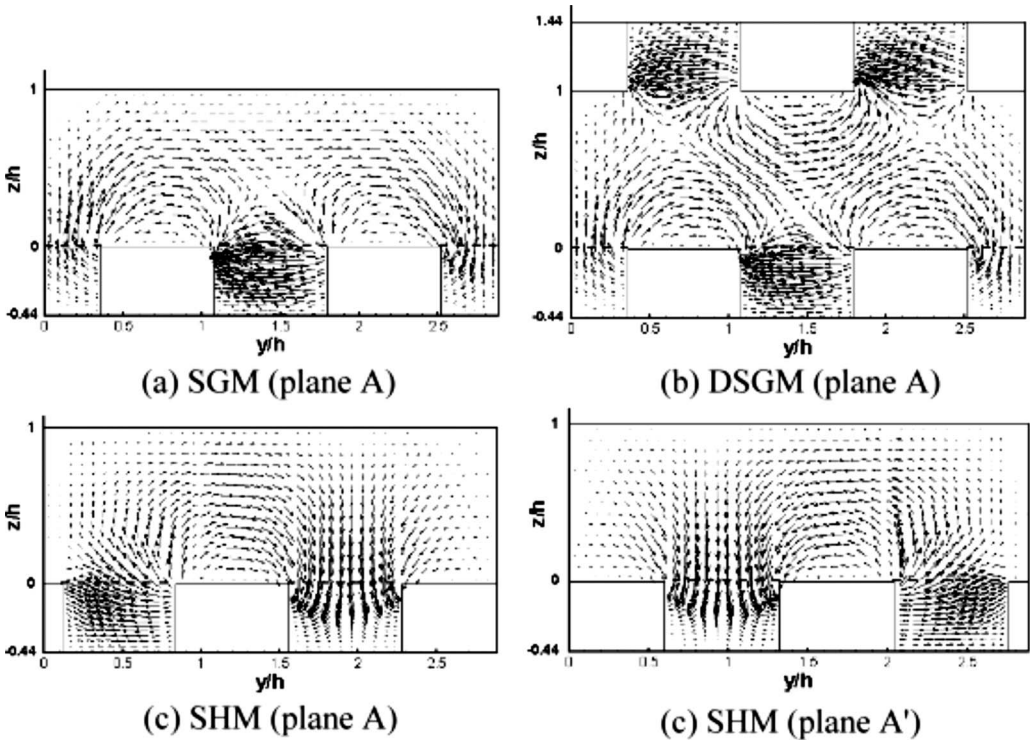

Fig. 4 Secondary velocity fields in cross sections for (*a*) SGM, (*b*) DSGM, and (*c*) SHM. The Planes A and A′ are referred to Fig. 1.

above the ridges. It is this secondary velocity resulting in helical streamlines in the channel [16]. It is evidenced from Fig. 5(*a*) that the two fluids, represented by two colors in blue and red, rotate in a clockwise sense during mixing evolution due to the transport by the helical flow. While the interface between the two fluids is twisted and, thus, elongated by the rotating flow, the sharp gradient in the interface is gradually smeared out by the molecular diffusion. To look into the mechanism causing the secondary flow, the projection of the velocity field onto the midplanes of a groove and a ridge (Planes B and C in Fig. 1) is given in Fig. 6. It appears that the flow in the floor region in Plane B is directed by the groove, followed by a returning flow along the top wall to form a perfect vortex flow rotating in the clockwise direction. The returning flow prevails in Plane C, which is located in the main passage of the channel.

For the DSGM, the staggered arrangement of the grooves on both walls induces a stronger secondary velocity in the channel core than that for the SGM, as shown in Fig. 4(*b*). The flow

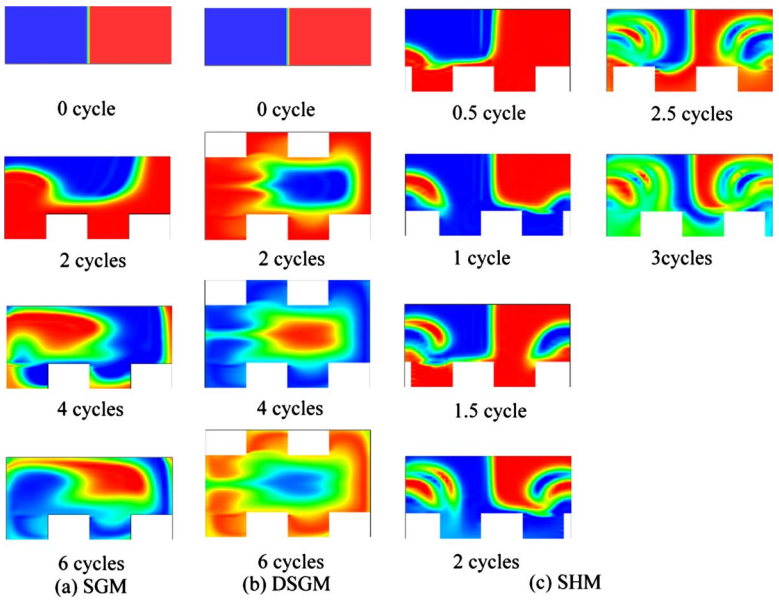

Fig. 5 Visualization of the concentration distribution in the *y-z* plane at different cycles for (*a*) SGM, (*b*) DSGM, and (*c*) SHM. Note that the length of a cycle for a SHM is longer than that for the SGM and DSGM.

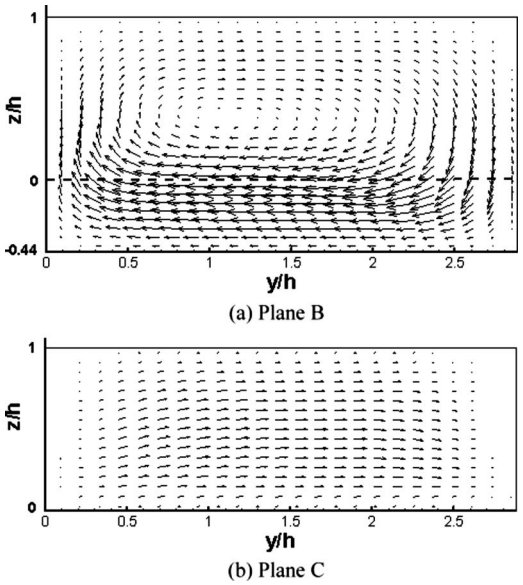

Fig. 6 Secondary velocity vectors in Planes B and C for the SGM. Plane B is a transversal plane in the middle of a groove and Plane C is located in the middle of a ridge. The locations of the planes are referred to Fig. 1. These planes are projected onto the *y-z* plane

rotates around both the upper and the lower ridges. The concentration plots given in Fig. 5(*b*) illustrate that in the beginning the fluid in blue is transported from the left to the right in the core region, while that in red fills up the grooves. It is followed by quick exchanges of the relative positions of the two fluids in the latter stage due to the secondary flow transportation. As a result, the mixing performance is enhanced when comparing with the SGM.

In the SHM, the asymmetry of the herringbone grooves with respect to the centerline brings about two circulating flows in different sizes, rotating in opposite directions. It is evident in Fig. 4(*c*) (Plane A) that the two flows merge at about $y/h=1.92$, which is the bending location of the herringbone grooves. In the second half of the cycle, the bending location together with the merging line shifts to $y/h=0.96$ (Plane A′) and the velocity field in the corresponding cross section changes accordingly to mirror the flow in the first half cycle. The mixing process is illustrated in Fig. 5(*c*) by presenting the concentration field every half a cycle until 3 cycles are completed. It is worthwhile to note that the mixing patterns shown have a strong resemblance to the fluorescent confocal micrographs of Stroock et al. [16]. The exchange of the two circulation patterns in each cycle causes the position change of the two fluids from one side of the cross section to the other side. After each exchange, part of one fluid is left to form an island being surrounded by the other fluid. The effects of this process can be more clearly identified by viewing the transversal plane at mid height of the channel. As seen in Fig. 7, the SHM functions like a lamination mixer [30,31], which constantly separates the flow into partial streams to form more and more laminae. Different from lamination mixers, the stratification of fluid is generated by the exchange of the circulation patterns in the SHM.

The mixing index shown in Fig. 8 implies that the SGM is a rather poor mixer. It could be seen from the Poincare map [20,21] that the flow behavior in the SGM is not really chaotic. The performance of this type of micromixer can be improved by using double grooves, as shown in the figure for the DSGM. Chaotic advection occurs in the SHM and its superiority is reflected in the plot.

The flow in the grooved microchannel and its performance depend strongly on the geometry of the groove. In the following, the

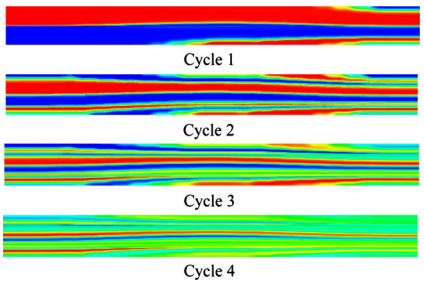

Fig. 7 Concentration filed in the *x-y* plane at mid height of the channel for the SHM

effects of the parameters such as the groove depth G_d, the groove width G_w, and the oblique angle of the groove α are examined for the SGM. The reference case has a groove depth of $0.44h$, a groove width of $0.72h$, and a groove angle of 45 deg. Totally, there are three kinds of depth ($G_d=0.2h$, $0.44h$, and $0.86h$) and three kinds of width ($G_w=0.36h$, $0.72h$, and $1.44h$) under consideration. Figures 9(*a*) and 9(*b*) reveal that the performance is enhanced with increasing values of groove depth and groove width. However, it does not mean that both can be enlarged without limits. There exist optimum values to maximize the mixing rate. This point can be demonstrated in Fig. 9(*c*). The mixing is enhanced by increasing the oblique angle from 30 deg through 45–60 deg. It is followed by a quick decline in performance when the angle is further increased to 75 deg. The improvement of the mixing is ascribed to the strengthening of the secondary flow. For demonstration, the transversal velocity along the channel height in the center of Planes B and C is presented in Fig. 10. It can be identified that a much stronger vortex flow is seen in the Groove Plane B for the oblique angles 45 deg and 60 deg. In the Ridge Plane C, the case with $\alpha=60$ deg has the greatest transversal velocity, which, in turn, leads to the fastest mixing.

Obstructed Micromixers. Another means to induce transversal flow is the use of obstacles to partly obstruct the microchannel. In grooved mixers, the grooves are carved on the bottom and/or top walls of the channel. Thus, the height of the channel is enlarged in the groove region. For obstructed mixers, block obstacles are inserted into the channel such that the width of the channel passage is reduced. Wang et al. [32] used a 2D numerical method to investigate the micromixer with cylindrical blocks placed in the channel. It was found that the asymmetric layouts of the obstacle are favored rather than the symmetric arrangements. The calculations of Wang et al. [33] showed that the mixing in a straight channel can be greatly enhanced by incorporating rectangular blocks within the micromixer. Bhagat et al. [34] examined the design of diamond-shaped blocks within a micromixer experimentally. They also reported simulated results for the flows with circular-shaped, triangular-shaped, diamond-shaped, and stepped-diamond-shaped blocks. Among them, the stepped-diamond-

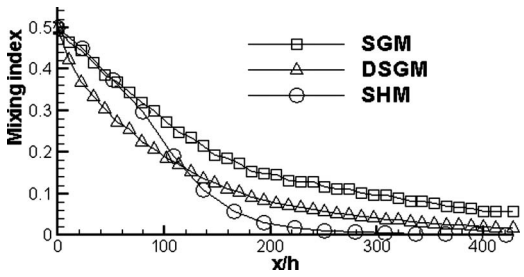

Fig. 8 Comparison of mixing performance for the SGM, DSGM, and SHM

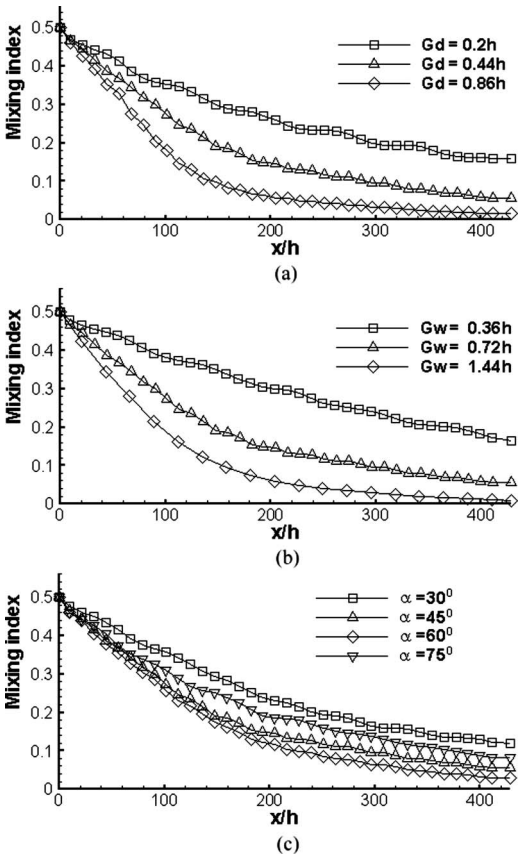

Fig. 9 Comparison of mixing performance for (*a*) different groove depths, (*b*) different groove widths, and (*c*) different oblique angles for the SGM

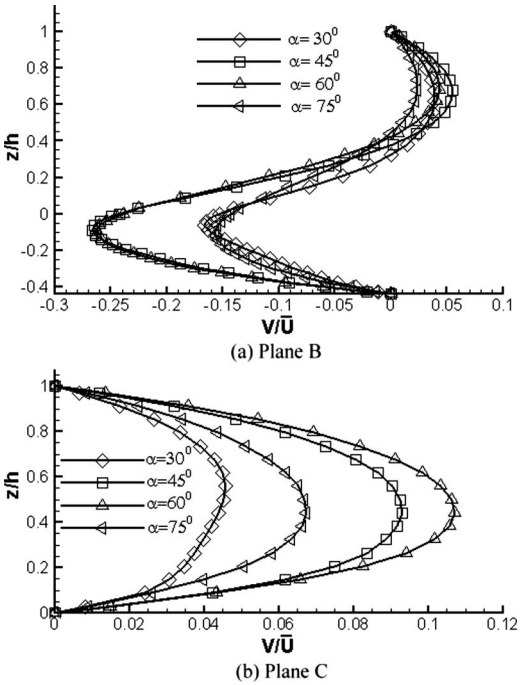

Fig. 10 Comparison of the transversal velocity along the vertical line in the center of Plane B and Plane C for different oblique angles. This transversal velocity is the component in the groove direction and is normalized by the inlet velocity $\bar{U}$.

shaped obstructions yield the best mixing.

In the above studies, the obstacles are placed in the core of the channel, away from the walls. An alternative way is to have obstacles intruding from the walls. In the following, we consider the micromixers with blocks being placed on the two side walls, arranged in a staggered manner, as shown in Figs. 1(*d*) and 1(*e*). The channel geometry of Fig. 1(*d*) is similar to the square-wave channel considered by Liu et al. [14]. The difference lies in the entrance and the outlet sections, which are of the same dimension as the wavy passage in the square-wave channel. In Fig. 1(*e*), the blocks are skew to the sidewalls, similar to the sawtooth structure investigated by Nichols et al. [35]. However, the sawtooth structure appeared only on one sidewall in their study. There are four types of arrangement in the present study (see Fig. 11). Types 1 and 3 are of rectangular type and the blocks of Types 2 and 4 are skew type with an oblique angle 45 deg to the walls. The block widths for Types 3 and 4 are half of those for Types 1 and 2 and the spaces between blocks are also reduced. The resulted mixing indices for Peclet numbers 2×10^5 and 2×10^3 are presented in Fig. 12. The results for the SGM and SHM are also included in the plots for comparison. For $\mathrm{Pe}=2\times10^5$, the performance of the block Type 1 is rather poor, being even worse than the SGM. The situation is much more improved in Type 2. The mixing performance is further enhanced by Types 3 and 4. Comparing with Type 3, Type 4 mixes the fluids a little faster in the initial stage. However, its mixing efficiency becomes slower for $x>0.5$ cm. As the Peclet number is reduced to 2×10^3 by decreasing the Reynolds number from 1 to 10^{-2}, the mixing rates for Types 1 and 3 are very similar to those for Types 2 and 4, respectively. It is of interest to note that at this extremely low Reynolds number even Types 1 and 2 perform better than the SHM.

The flow structure is illustrated in Fig. 13 for Types 1 and 2. Owing to the low velocity, flow separations are not detected at the sharp turnings and the corners formed by the blocks and the walls. It is noted that the two transversal passages in one period are not of the same width in the Type 2 channel. The narrower one has a width $w/2$, which is identical to that of the Type 1. However, the 45 deg oblique angle of Type 2 block results in higher flow velocity than Type 1. This explains the observation of higher mixing performance for the Type 2 at $\mathrm{Pe}=2\times10^5$. This advantage is lost when the importance of diffusion transport in the mixing process becomes more apparent as the Peclet number is reduced to 2×10^3. The evolution of the fluid mixing is illustrated in Fig. 14 for the four channel types. These obstructed channel flows are in essence two dimensional and, thus, nonchaotic because the vertical velocity component in the direction of the height is negligible. However, the great transversal velocity induced by the narrow passages in Types 3 and 4 leads to fast flow mixing. It may be claimed that the elongated passage length plays a more important role than the increased transversal velocity in the improvement of the mixing. In fact, the residence time of the fluid in these channels is not increased because the flow velocity is also greatly enlarged.

In the following, we compare the head losses for the considered micromixers. The variation of the mean pressure averaged over the cross section along the channel is shown in Fig. 15. The pressure shown is nondimensionalized by $\rho\bar{U}^2$. It is evident that in the macroscopic view, the pressure drops in a linear fashion along the channel. Note that there is a short intake duct at the inlet and an outlet duct at the exit, resulting in a piecewise linear variation of the curves. The grooved channels have almost the same pressure loss. The pressure gradients for SGM, SHM, and DSHM are −14.48, −14.35, and −13.65, respectively, for $\mathrm{Re}=1$ ($\mathrm{Pe}=2\times10^5$). The head loss is smaller for the DSHM because of the enlarged space by the double grooves. When the Reynolds number is reduced to 0.01 ($\mathrm{Pe}=2\times10^3$), the corresponding pressure gradients are increased by almost two orders. This result simply reflects the fact that the dimensionless head loss is inversely pro-

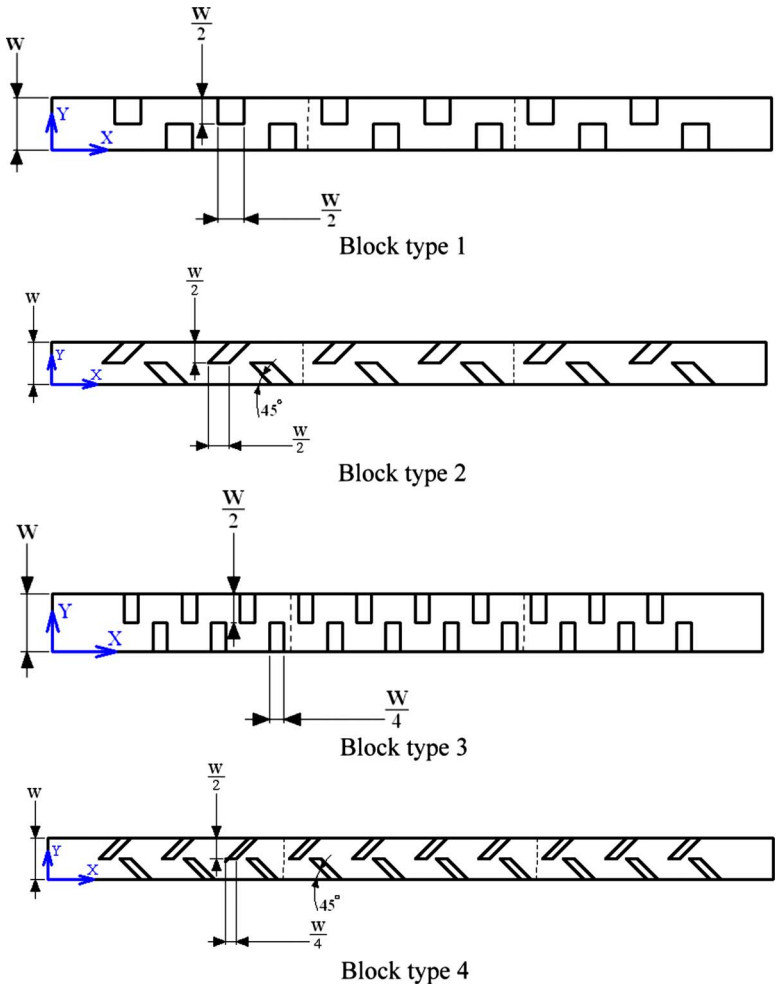

Fig. 11 Four types of block obstacles used in the obstructed microchannels

portional to the Reynolds number ($\Delta P/\rho \bar{U}^2 \sim 1/\mathrm{Re}$), which is expected in fully developed laminar flow. It can be identified from the figure that the blockage of the channel causes a large head loss. The slopes of the curves for Types 1–4 are −43.5, −41.1, −98.6, −90.5, respectively, which are about three to seven times as large as those for the grooved channels. It is interesting to note that the losses for Types 2 and 4 are slightly less than those for Types 1 and 3, respectively. This is attributed to that in a repeating period the second transversal passage between the blocks is much wider than the first one, which brings about a lower flow velocity and, thus, makes a pressure recovery.

4 Conclusions

A computational methodology has been developed to investigate the fluid mixing in microchannels. To make use of the periodic flow behavior, the calculation of velocity field is undertaken only in a part of the channel. With this cyclic velocity field, the evolution of the flow mixing throughout the channel can be monitored. Several mircomixers with either grooved channels or partially obstructed channels have been examined. Main findings are summarized in the following.

(1) For the microchannel with straight grooves (SGM), a well organized secondary vortex is induced in the groove plane. As a result, the flow in the channel features helical streamlines. Due to the helical flow, the interface between the fluids is distorted.
(2) By having grooves on both the top and the bottom walls,

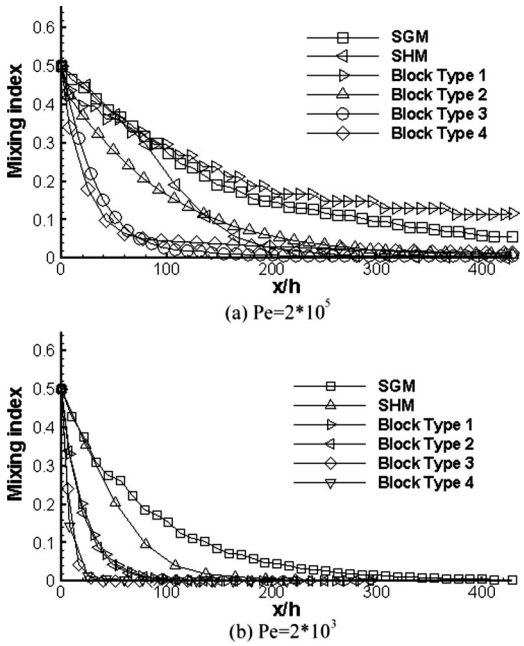

Fig. 12 Comparison of mixing performance for different block types: (*a*) Pe=2×10^5 and (*b*) Pe=2×10^3

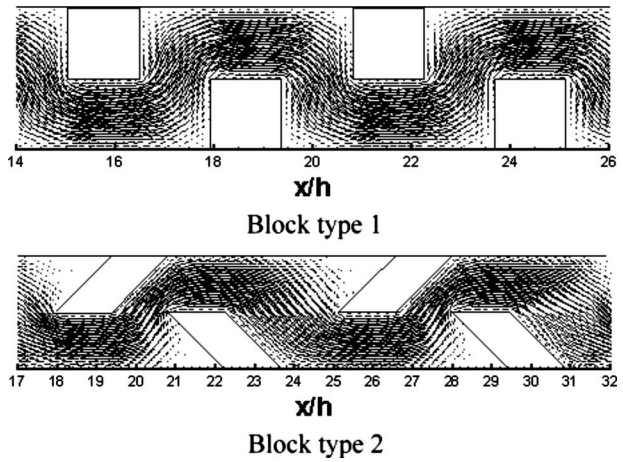

Fig. 13 Velocity field in the *x-y* plane at mid height of the channel for Block Types 1 and 2 at Pe=2×10^5

arranged in a staggered manner, the helical flow is greatly strengthened, leading to enhancement of the flow mixing.

(3) For the staggered herringbone microchannel, a pair of countervortices is created. The position exchange of the vortices results in stratification of the fluids. Consequently, a number of laminae are formed in the channel.

(4) The performance of the grooved micromixers can be improved by optimizing the geometric configuration of the groove. It was demonstrated for the SGM that with larger groove depths, groove widths, or oblique angles, the mixing is enhanced.

(5) The channel flows obstructed by blocks are indeed two dimensional. However, very strong transversal velocities can be produced via controlling the passage between the blocks to yield high mixing performance. However, this achievement is accompanied with a large pressure head loss.

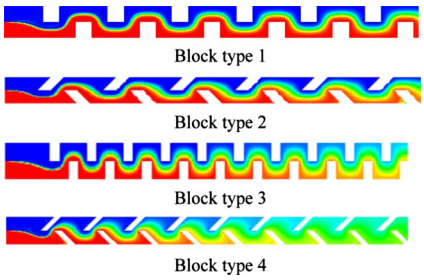

Fig. 14 Concentration field in the *x-y* plane at mid height of the channel for the four block types

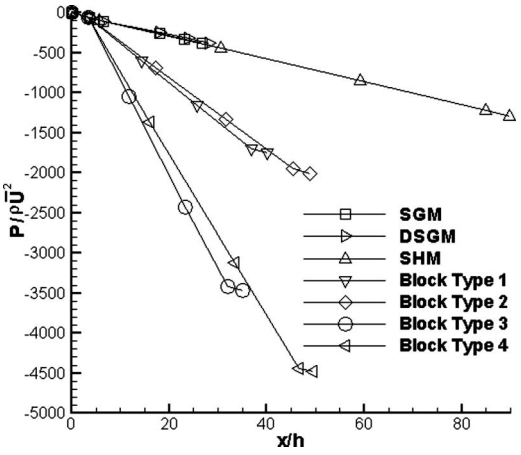

Fig. 15 Dimensionless pressure loss along the channel for all considered micromixers at Re=1 (Pe=2×10^5)

References

[1] Jacobson, S. C., McKnight, T. E., and Ramsey, J. M., 1999, "Microfluidic Devices for Electrokinetically Driven Parallel and Serial Mixing," Anal. Chem., **71**, pp. 4455–4459.

[2] Oddy, M. H., Santiago, J. G., and Mikkelsen, J. C., 2001, "Electrokinetic Instability Micromixing," Anal. Chem., **73**, pp. 5822–5832.

[3] Zhu, X., and Kim, E. S., 1998, "Microfluidic Motion Generation With Acoustic Waves," Sens. Actuators, A, **66**, pp. 355–360.

[4] Yang, Z., Matsumoto, S., Goto, H., Matsumoto, M., and Maeda, R., 2001, "Ultrasonic Micromixer for Microfluidic Systems," Sens. Actuators, A, **93**, pp. 266–272.

[5] Mao, H., Yang, T., and Cremer, P. S., 2002, "A Microfluidic Device with a Linear Temperature Gradient for Parallel and Combinatorial Measurements," J. Am. Chem. Soc., **124**(16), pp. 4432–4435.

[6] Tsai, J.-H., and Lin, L., 2002, "Active Microfluidic Mixer and Gas Bubble Filter Driven by Thermal Bubble Micropump," Sens. Actuators, A, **97–98**, pp. 665–671.

[7] Fujii, T., Sando, Y., Higashino, K., and Fujii, Y., 2003, "A Plug and Play Microfluidic Device," Lab Chip, **3**, pp. 193–197.

[8] Glasgow, I., and Aubry, N., 2003, "Enhancement of Microfluidic Mixing Using Time Pulsing," Lab Chip, **3**, pp. 114–120.

[9] Niu, X., and Lee, Y.-K., 2003, "Efficient Spatial-Temporal Chaotic Mixing in Microchannels," J. Micromech. Microeng., **13**, pp. 454–462.

[10] Ottino, J. M., 1989, *The Kinematics of Mixing: Stretching, Chaos, and Transport*, Cambridge University Press, Cambridge.

[11] Aref, H., 1984, "Stirring by Chaotic Advection," J. Fluid Mech., **143**, pp. 1–21.

[12] Aref, H., 2002, "The Development of Chaotic Advection," Phys. Fluids, **14**, pp. 1315–1325.

[13] Mengeaud, V., Josserand, J., and Girault, H. H., 2002, "Mixing Processes in a Zigzag Microchannel: Finite Element Simulation and Optical Study," Anal. Chem., **74**, pp. 4279–4286.

[14] Liu, R. H., Stremler, M. A., Sharp, K. V., Olsen, M. G., Santiago, J. G., Adrian, R. J., Aref, H., and Beebe, D. J., 2000, "Passive Mixing in a Three-Dimensional Serpentine Microchannel," J. Microelectromech. Syst., **9**, pp. 190–197.

[15] Stroock, A. D., Dertinger, S. K., Whitesides, G. M., and Ajdari, A., 2002, "Patterning Flows Using Grooved Surfaces," Anal. Chem., **74**, pp. 5306–5312.

[16] Stroock, A. D., Dertinger, S. K. W., Ajdarim, A., Mezic, I., Stone, H. A., and Whitesides, G. M., 2002, "Chaotic Mixer for Microchannels," Science, **295**, pp. 647–651.

[17] Johnson, T. J., Ross, D., and Locascio, L. E., 2002, "Rapid Microfluidic Mixing," Anal. Chem., **74**, pp. 45–51.

[18] Kim, D. S., Lee, S. W., Kwon, T. H., and Lee, S. S., 2004, "A Barrier Embedded Chaotic Micromixer," J. Micromech. Microeng., **14**, pp. 798–805.

[19] Howell, Jr., P. B., Mott, D. R., Fertig, S., Kaplan, C. R., Golden, J. P., Oran, E. S., and Ligler, F. S., 2005, "A Microfluidic Mixer with Grooves Placed on the Top and Bottom of the Channel," Lab Chip, **5**, pp. 524–530.

[20] Wang, H., Iovenitti, P., Harvey, E., and Masood, S., 2003, "Numerical Investigation of Mixing in Microchannels with Patterned Grooves," J. Micromech. Microeng., **13**, pp. 801–808.

[21] Kang, T. G., and Kwon, T. H., 2004, "Colored Particle Tracking Method for Mixing Analysis of Chaotic Micromixers," J. Micromech. Microeng., **14**, pp. 891–899.

[22] Mott, D. R., Howell, Jr., P. B., Golden, J. P., Kaplan, C. R., Ligler, F. S., and Oran, E. S., 2006, "A Lagrangian Advection Routine Applied to Microfluidic Component Design," *44th AIAA Aerospace Sciences Meeting and Exhibit*, AIAA Paper No. 2006-1086.

[23] Schonfeld, F., and Hardt, S., 2004, "Simulation of Helical Flows in Microchannels," AIChE J., **50**(4), pp. 771–778.

[24] Liu, Y. Z., Kim, B. J., and Sung, H. J., 2004, "Two-Fluid Mixing in a Microchannel," Int. J. Heat Fluid Flow, **25**, pp. 986–995.

[25] Tsui, Y.-Y., and Pan, Y.-F., 2006, "A Pressure-Correction Method for Incompressible Flows Using Unstructured Meshes," Numer. Heat Transfer, Part B, **49**, pp. 43–65.

[26] Tsui, Y.-Y., and Jung, S.-P., 2006, "Analysis of the Flow in Grooved Pumps with Specified Pressure Boundary Conditions," Vacuum, **81**, pp. 401–410.

[27] Patankar, S. V., Liu, C. H., and Sparrow, E. M., 1977, "Fully Developed Flow and Heat Transfer in Ducts Having Streamwise-Periodic Variations of Cross-Sectional Area," ASME J. Heat Transfer, **99**, pp. 180–186.

[28] Kelkar, K. M., and Patankar, S. V., 1987, "Numerical Prediction of Flow and Heat Transfer in a Parallel Plate Channel with Staggered Fins," ASME J. Heat Transfer, **109**, pp. 25–30.

[29] Murthy, J. Y., and Mathur, S., 1997, "Periodic Flow and Heat Transfer Using Unstructured Meshes," Int. J. Numer. Methods Fluids, **25**, pp. 659–677.

[30] Branebjerg, J., Gravesen, P., Krog, J. P., and Nielsen, C. R., 1996, "Fast Mixing by Lamination," *Proceedings of Ninth IEEE Int. Workshop on Micro Electro Mechanical Systems (MEMS'96)*, San Diego, CA, pp 441–446.

[31] Schonfeld, F., Hessel, V., and Hofmann, C., 2004, "An Optimized Split-and-

Recombine Micro-Mixer with Uniform 'Chaotic' Mixing," Lab Chip, **4**, pp. 65–69.
[32] Wang, H., Iovenitti, P., Harvey, E., and Masood, S., 2002, "Optimizing Layout of Obstacles for Enhanced Mixing in Microchannels," Smart Mater. Struct., **11**, pp. 662–667.
[33] Wang, R., Lin, J., and Li, H., 2007, "Chaotic Mixing on a Micromixer with Barriers Embedded," Chaos, Solitons Fractals, **33**, pp. 1362–1366.
[34] Bhagat, A. A. S., Peterson, E. T. K., and Papautsky, I., 2007, "A Passive Planar Micromixer with Obstructions for Mixing at Low Reynolds Numbers," J. Micromech. Microeng., **17**, pp. 1017–1024.
[35] Nichols, K. P., Ferullo, J. R., and Baeumner, A. J., 2006, "Recirculating, Passive Micromixer with a Novel Sawtooth Structure," Lab Chip, **6**, pp. 242–246.